XAFS study of local disorder in a-Gd_xSi_{1-x} amorphous magnetic semiconductor

D. Haskel[1], J. W. Freeland[1], J. Cross[2], R. Winarski[1], M. Newville[3], F. Hellman[4]
[1] *Advanced Photon Source, Argonne National Laboratory, Argonne IL 60439*
[2] *Pacific Northwest Consortium, University of Washington, Seattle, Washington 98195-1560*
[3] *Consortium for Advanced Radiation Sources, University of Chicago, Chicago IL 60637*
[4] *Department of Physics, University of California, San Diego, CA*

(January 14, 2003)

The local structure of amorphous a-Gd_xSi_{1-x} ($x = 0.04, 0.07, 0.12, 0.18$) magnetic semiconductor is determined from combined x-ray absorption fine structure (XAFS) measurements at the Gd L_3 and Si K absorption edges. XAFS data indicate that the structure is amorphous, with Gd atoms surrounded predominately by Si atoms, consistent with a random substitution of Gd in the Si network. Gd substitution induces a large local distortion resulting in a Gd-Si distance of 2.98(3) Å compared to a Si-Si distance of 2.39(1) Å. The lack of x dependence in the Gd local environment indicates that the distortions around the Gd do not interact with one another, even at $x = 0.18$. In addition, a small but systematic increase in mean squared disorder of Si-Si interatomic distance is observed with x. These results suggest that the amorphous Si network is very effective in relaxing the local strain through random displacements of Si atoms within a few Å of the perturbing Gd atoms.

I. INTRODUCTION

Amorphous magnetic semiconductors provide an excellent framework for studying the effect of local magnetic moments upon transport properties in the presence of disorder. It has been shown recently [1] that a-Gd_xSi_{1-x} exhibits a strong interaction between the Gd magnetic moments and the charge carriers. This interaction leads to localization of carriers at low temperature in zero field and results in large negative magneto-resistance in the presence of a magnetic field. The enhanced localization in zero field is believed to result from the random exchange interaction between disordered Gd moments and the carriers, shifting the mobility edge higher in the band and increasing the effective mass of the carriers. An applied field aligns the Gd magnetic moments resulting in spin polarization of the carriers, and lowering of the mobility edge leading to a field-induced insulator-metal transition at $x \approx 0.14$ [2,3]. Strong frustrated magnetic interactions between Gd moments lead to a spin glass freezing at low temperatures ($\lesssim$ 10K) and suppression of the magnetization below the non-interacting Brillouin function [1]. The magnetic susceptibility in the paramagnetic state shows a strong peak at the composition of the zero-field insulator-metal transition, indicative of polarization of carriers in a non-trivial way.

Since the interaction between highly localized Gd $4f$ moments is indirect; i.e., mediated by the carriers, its details depend on how the localization length (on the insulating side) or screening length (on the metallic side) of the carriers compares with the Gd-Gd interatomic distance. In this respect it is important to determine the local atomic environment around Gd atoms, as Gd clustering would strongly influence our understanding of both transport and magnetization properties, typically leading to ferromagnetic clusters and hopping conductivity from cluster to cluster. It has been argued on the basis of magnetic measurements [1–3] and local density functional theoretical simulations of the non-magnetic analog a-Y_xSi_{1-x} [4] that clustering does not occur. It is clear however that direct structural characterization of magnetic amorphous semiconductors at the atomic scale is of paramount importance for understanding their magnetic and electronic properties.

Here we report on the use of x-ray absorption fine structure (XAFS) technique [5] to study the local structure around Gd and Si atoms. Since XAFS is only sensitive to short range order in the atomic arrangement and does not require long range crystalline order it is ideally suited for the study of local structure in amorphous materials [6]. In addition, XAFS is element specific; i.e., it measures the *partial* pair distribution function between an absorber and its neighbors, so it can be used to independently determine the local structure about Gd and Si atoms. Other powerful probes of local structure, such as the pair distribution function analysis of neutron and x-ray scattering data [7,8], measure a sum over *all* pair correlations which includes only a small contribution from dilute dopants. XAFS completely isolates the local structure around the dopants. In this work, we exploit these features of XAFS to independently determine the local structure around the Gd and Si atoms in a-Gd_xSi_{1-x} with x=0.04, 0.07, 0.12 and 0.18.

II. EXPERIMENTAL

Samples used in this study were thin films (≈ 1000 Å) grown by electron beam co-evaporation from separately controlled Si and Gd sources in an ultra high vacuum deposition system (base pressure 2×10^{-10} Torr). Samples were grown onto amorphous silicon-nitride coated Si substrates held near room temperature during growth (below 80°C). The deposition rate was approximately 1 Å/sec and the pressure of the chamber during growth was below $1{\times}10^{-8}$ Torr. Transmission electron microscopy (TEM) measurements of thin (300 Å) samples grown on silicon nitride windows and X-ray diffraction analysis of thicker (1000-4000 Å) samples show an amorphous structure with no discernible crystallinity. A columnar microstructure is visible in the TEM images, as is commonly observed in amorphous materials prepared by e-beam evaporation. Compositions and atomic areal density (Gd and Si atoms/cm^2) were determined by Rutherford Backscattering (RBS); thickness was determined by Dektak profilometry. RBS shows no measurable oxygen or other impurities in any of these electron beam evaporated films, which sets an upper limit of approximately 1 at.% oxygen or other contamination. Magnetization, magnetotransport, tunneling spectroscopy, IR absorption spectroscopy and specific heat have been measured on samples prepared in the same system (in some cases, on the same samples presented here); these results are described in refs. 1–3, 9, 10. Samples are stable in air (even with no capping layer) and show no sign of structural relaxation or significant oxidation even after several years. Detailed characterization of native oxide formation has not been performed, but tunnel junctions formed by deposition of a Pb counterelectrode show that a thin native oxide (tunnel resistance of order 1 kΩ, hence thickness of order 20 Å) forms quickly (within an hour) on the alloy surface. Storage at room temperature in air for a year or more results in a tunnel resistance of order 1 MΩ, indicating formation of a thicker native oxide (thickness of order 30-100 Å), but samples remain visibly shiny and metallic, and show no significant change in any property (conductivity or magnetization, both of which should be sensitive to clustering or structural changes). Gd-Si thus appear to be remarkably stable in air and resistant to structural relaxation, despite the high proportion of rare earth. By contrast, amorphous Tb-Fe alloys of comparable rare earth composition visibly oxidize within a short period of time, and Gd-Ge alloys show signs of significant structural relaxation at room temperature.

XAFS measurements at the Gd L_3 edge ($2p_{3/2}$ excitation) were performed at beamline 20-BM of the PNC-CAT at the Advanced Photon Source using Si (111) double crystal monochromators resulting in ≈ 1 eV energy resolution at an incoming energy of 7.243 keV. Data was collected in fluorescence geometry using a single element Ge solid state detector. The samples were cooled to T=12K in a He-flow cryostat to reduce thermal vibrations, which decrease the XAFS amplitude. XAFS measurements at the Si K-edge ($1s$ excitation) were performed at beamline 4-ID-C of the SRI-CAT at the Advanced Photon Source. A grating monochromator with 600 lines/mm was used resulting in ≈ 1.2 eV energy resolution at an incoming energy of 1.83 keV. Samples were sputtered at room temperature *in-situ* with Ar for 1-2 hours prior to the measurements in order to remove any surface oxide passive layer. The chamber base pressure during the measurements was 10^{-9} Torr and data were collected at room temperature in the total electron yield mode. X-ray absorption near-edge structure (XANES) measurements were also carried out near Gd $M_{2,3,4,5}$ absorption edges, indicating a Gd^{3+} valence state [11].

III. RESULTS AND DISCUSSION

A. General remarks

The cross section for photoelectric x-ray absorption past an absorption edge of a deep core atomic state in condensed matter exhibits energy dependent fine structure due to modification of the photoelectron (p.e.) final state (at the position of the absorbing atom) introduced by scattering from neighboring atoms. For K-edges ($1s$) in single scattering (SS) and harmonic approximations, this fine structure (XAFS) is given by [5, 12]

$$\chi(k) = -\sum_j 3(\hat{\epsilon}\cdot\hat{r_j})^2 \frac{S_0^2 N_j F_j(\pi,k,r_j)}{k r_j^2} e^{-2k^2\sigma_j^2} \times e^{-2r_j/\lambda(k)} \sin(2kr_j + \delta_j(k,r_j)), \quad (1)$$

where k is the p.e. wavenumber measured relative to the Fermi level, $S_0^2 N_j$ an effective coordination number which includes changes in the passive electrons' wave functions due to the presence of the core hole, F_j a spherical wave backscattering amplitude, σ_j the root mean squared relative displacement in interatomic distance, λ an effective mean free path which includes the finite lifetime of the core hole, r_j the interatomic distance, δ_j an overall scattering phase shift and $\hat{\epsilon}$ the x-rays' polarization vector. The sum is over all possible single scattering paths. For evaporated films with no preferred orientational ordering an angular averaging over the relative orientations of electric field vector of the linearly polarized synchrotron radiation and the bond direction gives $\langle(\hat{\epsilon}\cdot\hat{r_j})^2\rangle$=1/3 and the XAFS only contains information on the radial part of the partial pair distribution function. Since the XAFS is a superposition of oscillatory functions in p.e. momentum space, a Fourier transform (FT) of $\chi(k)$ with respect to $2k$ is related to this pair distribution function about the absorbing atom but "peaks" in this FT appear shifted from the actual interatomic distances due to the k-dependence of the total p.e. phase shift $\delta_j(k)$ in eq. 1. In the absence of angular dependence the XAFS expression at the L_3 edge is essentially the same as that in eq. 1 except that the phase shift is modified to account for the d-symmetry of the final state [13].

The experimental XAFS, $\chi^{\rm exp}(k)$, is obtained after subtracting the embedded-atom absorption background from the measured absorption coefficient [14] and normalizing by the edge step; namely $\chi^{\rm exp}(k)$=$[\mu(k)-\mu_0(k)]/\Delta\mu_0(0)$. The photoelectron wavenumber k is defined by $k=\sqrt{2m(E-E_0)/\hbar^2}$, where E is the photon energy and E_0 is the absorption threshold for a core electron excitation, selected to be near the midpoint of the edge step. The data were analyzed using the UWXAFS analysis package [15] together with theoretical standards from FEFF6 [16], the latter used to calculate $F_j(k), \delta_j(k), \lambda(k)$. A theoretical $\chi^{\rm th}(k)$ is constructed whose adjustable structural parameters r_j, N_j, σ^2 are refined against the experimental data by non-linear least squares minimization of a reduced χ^2_ν statistic [15],

$$\chi^2_\nu = \frac{N_I}{\nu N}\sum_{i=1}^{N}\left(\frac{\left|\tilde{\chi}^{\rm th}(r_i)-\tilde{\chi}^{\rm exp}(r_i)\right|}{\epsilon(r_i)}\right)^2, \qquad (2)$$

where the sum is over all pairs of points (real and imaginary parts of the difference are evaluated) in the fitted region of Fourier transformed r-space. Here $N_I=(2\Delta k\Delta r)/\pi+2$ is the number of independent points in the fitted region [17], $\nu=N_I-N_P$ the degrees of freedom in the fit and $\epsilon(r_i)$ the evaluated uncertainty in the numerator's difference of Eq. 2. An estimate for ϵ is obtained from the rms value of $\chi^{exp}(r)$ in the range [15,25] Å, where the XAFS is indistinguishable from the random noise. This underestimates the uncertainty since it does not include systematic errors in the data and theory. Whereas a good fit should result in $\chi^2_\nu\approx 1\pm\sqrt{2/\nu}$ [15,18], a miss-evaluation of ϵ causes χ^2_ν to miss-represent the quality of the fit, typically resulting in $\chi^2_\nu\gg 1$. In order to properly include the effects of both systematic and random errors a fractional misfit R is evaluated [18],

$$R=\frac{\sum_{i=1}^{N}\left|\tilde{\chi}^{\rm th}(r_i)-\tilde{\chi}^{\rm exp}(r_i)\right|^2}{\sum_{i=1}^{N}\left|\tilde{\chi}^{\rm exp}(r_i)\right|^2}. \qquad (3)$$

A small value of R together with $\chi^2_\nu\gg 1$ indicates that systematic errors dominate the uncertainty and rescaling $\epsilon\rightarrow\epsilon\sqrt{\chi^2_\nu}$ recovers the $\chi^2_\nu\approx 1$ criteria for a good fit. Uncertainties in the parameters, which are calculated by the change needed to increase χ^2_ν by $1/\nu$ from its minimum value (1 standard deviation) and which include the effect of correlations between fitting parameters, are rescaled by $\sqrt{\chi^2_\nu}$. An overall E_0 shift fitting parameter is used to adjust the $k=0$ reference between experiment and theory. The former is arbitrarily selected to be near the midpoint of the absorption edge.

B. Local structure at Gd sites

Figure 1 shows raw absorption data at the Gd L_3 edge for a $Gd_{0.18}Si_{0.82}$ sample at T=12K together with the background function used to simulate the embedded atom absorption. The resultant XAFS data, averaged over 12 consecutive scans, is also shown. The measured random noise in the XAFS data, obtained from the averaged rms variation between consecutive scans, is $\sim 2\times 10^{-2}$, limiting the usable upper k-range to about $7\,\text{Å}^{-1}$. Uncertainties in background removal limit the k-range from below to about $2\,\text{Å}^{-1}$. Since the background function was defined to include frequencies up to 1.2 Å [14], XAFS data in the $\Delta k=[2-7]\,\text{Å}^{-1}$ range was Fourier transformed to real space and fitted in the range $\Delta r=[1.5-3]$ Å, which includes first shell information only. The total number of independent points in this fitting range is $N_I=8$ while only a total of four fitting parameters are used. Correlations between $(E_0,\delta r_j)$ and (N_j,σ^2) fitting parameters were reduced by weighting the XAFS data by $k^w(w=1,2,3)$ and simultaneously fitting the differently weighted XAFS, $k^w\chi(k)$, using a single set of structural parameters. This assures that the values obtained for the fitting parameters are physical; i.e., they do not depend on the arbitrary k-weight used in the analysis. We note that our error analysis includes the effect of correlations between the fitting parameters mentioned above.

Figure 2 shows the magnitude and real part of the complex Fourier transform together with fits to the data. The passive electron amplitude reduction factor, which is assumed to depend only on the absorbing atom type and not on its environment [19], was obtained from fits to Gd metal foil data as $S_0^2=0.76(5)$ and set to this value in all other fits. Structural parameters derived from best fits are shown in table I. Our best fits were achieved for a first shell coordination composed of only Si atoms. The measured Gd-Si distance is 2.98(3) Å, nearly independent of x (table I). For comparison, the fitted Si-Si distance in the same samples is 2.39(1), Å and the fitted Gd-Gd distance in the Gd metal foil is 3.550(8) Å. Allowing for partial Gd coordination near the first shell distance of ≈ 3.0 Å results in poorer fit quality by about a factor of three (given by χ^2_ν and R) and a fitted coordination of 0 ± 0.9, independent of Gd concentration. This is not surprising since atomic size arguments will suggest a longer Gd-Gd distance. We note that Gd and Si backscattering amplitudes and phases differ significantly in the k-range used in the analysis which allows distinguishing these neighboring atom types. Since the large degree of disorder results in no measurable second shell XAFS above the noise, information on Gd-Gd pair correlations near the Gd-Gd metallic distance of ≈ 3.6 Å cannot be obtained.

Despite no indication of oxygen presence in our samples the possibility of undesired oxygen impurities coordinating the Gd atoms was considered in light of the observation that Er implanted silicon tends to exhibit a Er_2O_3 local structure [20]. Similarly, a Gd_2O_3 local structure would be expected based on the Gd^{3+} valence state. The measured first shell distance of nearly 3.0 Å rules out the presence of oxygen coordination, as the latter has a much shorter Gd-O bonding distance of about 2.35 Å [21]

Since the orientational arrangement of atoms in the first shell cannot be resolved, this measurement does not provide information on whether Gd atoms substitute at the tetrahedrally coordinated sites of the amorphous Si network or reside in interstitial cavities as found for Y in *a*-YSi [4]. In any event it is clear that Gd is predominately coordinated by Si. Although the most likely answer is no Gd neighbors at or near the Gd-Si first shell distance, our error bars allow up to $\approx 16\%$ Gd-Gd neighbors in the first shell. While this is consistent with a model in which Gd is randomly distributed in the Si network up to $x = 0.18$, one cannot rule out the presence of very small amounts of Gd clusters. Assuming metallic-like clusters (coordination of 12) this sets an upper limit of about 1-2% for the fractional volume of Gd in metallic clusters.

C. Local structure at Si sites

Figure 3 shows raw absorption data at the Si K edge of a $Gd_{0.18}Si_{0.82}$ sample at T=300K together with the embedded atom background function and the resultant XAFS data. The measured random noise in the XAFS data is $\sim 5 \times 10^{-3}$. Data in the $k = [2-8]$ Å^{-1} range was Fourier transformed and fitted in real space in the $\Delta r = [1.2-3]$ Å range. The total number of independent points is $N_I \sim 9$ while the total number of fitting parameters used was five. In this case the background function was defined to include frequencies of up to 1 Å.

Best fits are shown in Figure 4 and the refined structural parameters are summarized in table II. Best fits were obtained for a first shell coordination composed of only Si atoms. The correlations between coordination number N and σ^2 fitting parameters were reduced by simultaneously fitting differently k-weighted data with the same set of structural parameters. In this manner, we were able to determine that the reduction in the first shell XAFS amplitude with x (inset b in fig. 4) is due to an increased disorder in the Si-Si interatomic distance with Gd doping and not due to a decrease in coordination about Si atoms, as summarized in table II. The mean squared disorder, σ^2, systematically increases from 0.0048(9) Å^2 at $x = 0.04$ to 0.008(1) Å^2 at x=0.18. We found no deviation from a Gaussian distribution of Si-Si interatomic distances within the resolution of our measurements.

The measured Si-Si average distance is 2.39(1) Å and the measured average coordination number is $N = 3.7(3)$. The variation in these numbers with x is smaller than their uncertainties. These values are in excellent agreement with the 3.79(1) coordination obtained for pure *a*-Si by PDF analysis of high energy x-ray diffraction data [8]. The root mean-squared variation in Si-Si distance (σ) extrapolated to $x = 0$ is $\sigma = 0.06(2)$ Å in good agreement with the value of $\sigma = 0.064(1)$ Å obtained in the pair distribution function (PDF) analysis of pure *a*-Si [8]. The Si-Si average distance is ≈ 0.04 Å longer than the 2.35 Å Si-Si distance in crystalline Si. This does not depend on Gd doping so this expansion is intrinsic to the amorphous Si network. A similar Si-Si average distance is observed in molecular dynamics simulations of pure *a*-Si [22] and sizable increases in bond length are also measured by XAFS in pure *a*-Ge [23]. No significant increase in bond length, however, was detected in the PDF study of ref. 8. As discussed in the literature (e.g., see refs. 8, 22 and references therein) evaporated *a*-Si films might exhibit different concentrations and types of defects than those present in the ion-implanted *c*-Si used in ref. 8. For the case here, where local structure information is sought to shed light into the remarkable magnetic properties of *a*-Gd_xSi_{1-x}, it is critical that the XAFS measurements were done on samples whose magnetic properties were thoroughly characterized [1, 3].

Attempts to include Gd atoms near the first coordination shell distance of ≈ 2.4 Å resulted in significantly poorer fits and a fitted Gd coordination of 0 ± 0.5. The Si-Gd correlations occur at the much longer distance of ≈ 3.0 Å (beyond first shell) as determined for Gd-Si in the Gd XAFS analysis. Attempts to retrieve information on Si-Gd correlations near this distance resulted in a fitted Gd coordination of 0 ± 0.7. The error bar is consistent with up to 18% presence of Gd in the first two coordination shells of Si.

IV. DISCUSSION

As seen in table I the local environment about Gd atoms is nearly independent of Gd concentration. This implies that the strain field about Gd dopants is confined to very short distances. One can estimate the extent of this confinement by noticing that, for a random distribution of dopants, the average Gd-Gd interatomic separation is at least $\approx 2.98x^{-1/3}$ or 5.27 Å at $x = 0.18$. For the local distortions around Gd dopants to be isolated from each other it requires that their characteristic length scale be smaller than half this average separation, or about 2.6 Å, which limits the spatial extent of the distortion field to the first coordination shell. Alternatively, one can use a second shell distance of 3.84 Å in crystalline Si instead of the measured Gd-Si distance of 2.98 Å as the minimum Gd-Gd separation. This yields a Gd-Gd average separation of 6.8 Å at $x = 0.18$, limiting the distortion field to about 3.4 Å. These two limiting cases give a possible range of the strain field between 2.6 and 3.4 Å, mostly confined to within the first coordination shell.

The increased mean squared disorder in Si-Si distance with increased Gd doping (table II) is not surprising since Gd locally expands its immediate surroundings. Increasing its concentration simply increases the number of Si atoms that are randomly displaced from their average positions in order to accommodate the local strain. A random distribution of Gd dopants results in random displacements of Si atoms in their vicinity. These random displacements lead to enhanced mean squared variations in Si-Si interatomic distance while on average this distance remains nearly unchanged. We note that despite the relatively large Gd concentration at $x = 0.18$ the overall increase in mean squared disorder is not large in an absolute scale (table II). Comparable increases in σ^2 are commonly observed in crystalline materials due to increased lattice vibrations at 300K compared to 10K [24]. This small increase in disorder is consistent with the idea that the Si amorphous network acts quite efficiently in relaxing the local strain around Gd dopants.

Special emphasis was placed in the determination of coordination number about Si atoms as function of Gd doping. This was motivated by results from density functional-based molecular dynamics simulations of the non-magnetic analog a-Y_xSi_{1-x}, which show that Y doping introduces Si dangling bonds in its immediate vecinity leading to low coordinated Si atoms [4]. If a similar effect occurs in a-GdSi, it should manifest itself in the XAFS as a systematic decrease, with doping, in the measured coordination number about Si atoms. We took special care to properly account for the effect of correlations between N and σ^2 fitting parameters. Although N and σ^2 affect the XAFS amplitude in different ways (constant versus k-dependent contributions), a miss-evaluation of N can be partially compensated by a change in σ^2, especially when data is available over a short k-range. These correlations between fitting parameters cannot be completely removed, but they can be affected by weighting the data by different k-weights. Since σ^2 has a larger effect on the data at high k, k-weighting should result in a more accurate determination of σ^2. On the other hand, the XAFS signal to noise ratio is smaller at high k and k-weighting will tend to emphasize this noise. It is clear that the true physical parameters cannot depend on the arbitrary k-weighting of the data. Our approach is then to simultaneously fit differently k-weighted data with the same set of variable structural parameters.

To illustrate this point we show in figure 5 fitted values of N obtained for different values of σ^2 *set* in the interval [0.001, 0.01] Å^2. This is done for different k-weighting of the data. Large error bars in the fitted value of N correspond to poor quality fits. It is clear that *for a given k-weight* changes in σ^2 over certain range can be accommodated by corresponding changes in N without significantly affecting the fit quality (seen by similar size of error bars). These correlations, however, change with k-weight and result in different fitted values of N for a given σ^2, as shown in figure 5. The physical N should not depend on the arbitrary k-weight used in the analysis and can be found at the intersection point of the different k-weights. The results for $x = 0.04$ and $x = 0.18$ indicate that there is a significant increase in σ^2 with Gd doping while the coordination number N remains constant. Results from the nearly equivalent procedure of simultaneous fits of differently weighted XAFS data in table II support this conclusion. We note that preliminary XAFS data taken at the Y K-edge of a-$Y_{0.17}Si_{0.83}$ at room temperature give a Y-Si distance of 2.90(3) Å, ≈ 0.1 Å shorter than the Gd-Si distance. The shorter distance in the former case might facilitate charge transfer from the Y^{+3} ions to its Si neighbors and related formation of Si dangling bonds [4]. XAFS experiments at the Si K-edge of a-$Y_{1-x}Si_x$ are being planned to further assess this question.

V. SUMMARY AND CONCLUSIONS

Using XAFS as a local structural probe we have determined the local atomic environment about Gd and Si atoms in amorphous Gd_xSi_{1-x} magnetic semiconductor. Gd doping introduces a large local distortion in its immediate environment resulting in a Gd-Si distance ≈ 0.6 Å longer than the Si-Si distance. This local strain is accommodated by increased disorder in the Si network in the form of random atomic displacements. The strain around Gd dopants is efficiently relaxed at very short distances, with the induced atomic displacements mostly confined to the first coordination shell of Si atoms around Gd dopants. The superior ability of the network to relax the strain field at such short distances is likely due to its amorphous nature. Although there is a systematic increase, with doping, in the amount of static disorder in the Si network, the overall increase is relatively small, again reflecting the ability of the Si network to accommodate the local strain around Gd ions.

Although XAFS in a disordered system can not resolve the orientational arrangement of atoms in the first coordination shell, a coordination of about four strongly suggests a local tetrahedral environment for Si. Whether Gd substitutes at the sites of the amorphous Si network or sit at network cavities as found for Y in a-YSi [4] cannot be resolved from these measurements. We cannot rule out a larger coordination around Gd sites consistent with our uncertainties.

We found no evidence for Gd clustering in our data, which shows that Gd is predominately coordinated by Si. Our uncertainties, however, allow for up to $\approx$ 18% Gd-Gd and Si-Gd neighbors near the first shell distance consistent with a random distribution of Gd in the Si network. The possibility of minor amounts of Gd metallic clusters (coordination of 12) cannot be ruled out from the XAFS measurements, but an upper limit of about 1-2% can be set for the fractional volume of Gd in such metallic clusters. This is consistent with Curie-Weiss law fits to magnetic susceptibility data [1], $\chi = A/(T-\theta)$, which show near-zero values of θ ($\lesssim 2.5$ K) for all samples and no significant curvature in the $1/\chi$ data at any temperature, both indicative that no significant ferromagnetic ordering due to clustering is present.

The random distribution of dopants constrains the minimum average separation between Gd dopants to $\gtrsim 5.27$ Å. This is much larger than the Gd-Gd distance in Gd metal and has to be considered when addressing the origin of large negative magneto-resistance in these alloys.

VI. ACKNOWLEDGMENTS

We acknowledge the valuable help of S. W. Han with the XAFS experiments, B. L. Zink with sample preparation and R. Culbertson for assistance with RBS analysis. DH benefited from helpful discussions with Dr. B. Ravel. Work at Argonne is supported by the U. S. DOE, Office of Science, under Contract No. W-31-109-ENG-38. FH thanks the NSF for support (DMR 97-05300 and 02-03907).

[1] F. Hellman, M. Q. Tran, A. E. Gebala, E. M. Wilcox, and R. C. Dynes, Phys. Rev. Lett. **77**, 4652 (1996); F. Hellman, D. R. Queen, R. M. Potok, and B. L. Zink, *ibid* **84**, 5411 (2000).
[2] P. Xiong, B. L. Zink, S. I. Applebaum, F. Hellman, and R. C. Dynes, Phys. Rev. B **59**, R3929 (1999).
[3] W. Teizer, F. Hellman, and R. C. Dynes, Sol. St. Comm. **114**, 81 (2000); W. Teizer, F. Hellman, and R. C. Dynes, Phys. Rev. Lett. **85**, 848 (2000).
[4] V. Meregalli and M. Parrinello, Sol. St. Comm. **117**, 441 (2001).
[5] E. A. Stern, Phys. Rev. B **10**, 3027 (1974).
[6] A. N. Mansour *et al.*, Phys. Rev. B **65**, 134207 (2002); G. Dalba *et al.*, Physics and Chemistry of Glasses **41**, 290 (2000); T. Watanabe *et al.*, Jpn. J. Appl. Phys. 1 **38**, 516 (1999); M. Majid *et al.*, Phys. Rev. B **58**, 6104 (1998); A. Frenkel *et al.*, *ibid* **54**, 884 (1996); J. B. Kortright and A. Bienenstock, Phys. Rev. B **37**, 2979 (1988).
[7] T. Egami, H. D. Rosenfeld, B. H. Toby, A. Bhalla, Ferroelectrics **120**, 11 (1991).
[8] K. Laaziri, S. Kycia, S. Roorda, M. Chicoine, J. L. Robertson, J. Wang and S. C. Moss, Phys. Rev. B **60**, 13520 (1999); K. Laaziri, S. Kycia, S. Roorda, M. Chicoine, J. L. Robertson, J. Wang and S. C. Moss, Phys. Rev. Lett. **82**, 3460 (1999).
[9] D. N. Basov *et al.*, Europhys. Lett. **57**, 240 (2002).
[10] B. L. Zink, E. Janod, K. Allen, and F. Hellman, Phys. Rev. Lett. **83**, 2266 (1999).
[11] F. Hellman *et al.*, to be published.
[12] P. A. Lee and J. B. Pendry, Phys. Rev. B 11, 2795 (1975).
[13] S. M. Heald and E. A. Stern, Phys. Rev. B **16**, 5549 (1977).
[14] M. Newville. P. Livins, Y. Yacoby, J. J. Rehr, and E. A. Stern, Phys. Rev. B **47**, 14126 (1993).
[15] E. A. Stern, M. Newville, B. Ravel, Y. Yacoby, and D. Haskel, Physica B **208&209**, 117 (1995).
[16] S. Zabinsky, J. J. Rehr, A. Ankudinov, R. C. Albers and M. J. Eller, Phys. Rev. B **52**, 2995 (1995).
[17] E. A. Stern, Phys. Rev. B **48**, 9825 (1993).
[18] M. Newville, B. Ravel, D. Haskel, J. J. Rehr, E. A. Stern and Y. Yacoby, Physica B **208&209**, 154 (1995).
[19] J. J. Rehr, E. A. Stern, R. L. Martin and E. R. Davidson, Phys. Rev. B **17**, 560 (1978); E. A. Stern, B. A. Bunker and S. M. Heald, Phys. Rev. B **21**, 5521 (1980).
[20] M. A. Marcus and A. Polman, J. non-crystal. sol. **136**, 260 (1991); L. R. Tessler *et al.*, J. non-crystal. sol.**299-302**, 673 (2002).
[21] Z. Heiba, H. Okuyucu, and Y. S. Hascicek, J. Appl. Cryst. **35**, 577 (2002).
[22] J. Nord, K. Nordlund, and J. Keinonen, Phys. Rev. B **65**, 165329 (2002).
[23] C. J. Glover, M. C. Ridgway, K. M. Yu, G. J. Foran, C. Clear, J. L. Hansen, and A. Nylandsted-Larsen, Phys. Rev. B **63**, 073204 (2001).
[24] D. Haskel, E. A. Stern, V. Polinger and F. Dogan, Phys. Rev. B **64**, 104510 (2001).

TABLE I. Structural parameters for Gd-Si distance in a-Gd_xSi_{1-x} at T=12K. Number of independent points is $N_I = 8$ and number of fitting parameters $N_P = 4$; $S_0^2 = 0.76(5)$.

x	r(Å)	σ^2(Å^2)	N	χ^2_ν	R
0.07	2.98(1)	0.006(3)	4.8 (1.1)	10.1	0.04
0.12	2.97(1)	0.005(3)	4.5 (1.2)	9.0	0.03
0.18	2.99(1)	0.007(2)	4.7 (1.0)	11.5	0.05

TABLE II. Structural parameters for Si-Si distance in a-Gd_xSi_{1-x} at T=300K. Number of independent points is $N_I = 9$ and number of fitting parameters is $N_P = 5$; $S_0^2 = 0.7(1)$

x	r(Å)	σ^2(Å^2)	N	χ^2_ν	R
0.04	2.385(5)	0.0048(09)	3.7 (0.3)	22	0.007
0.07	2.386(8)	0.0059(12)	3.8 (0.4)	29	0.017
0.12	2.392(4)	0.0071(06)	3.6 (0.3)	28	0.010
0.18	2.390(6)	0.0080(13)	3.7 (0.3)	32	0.014

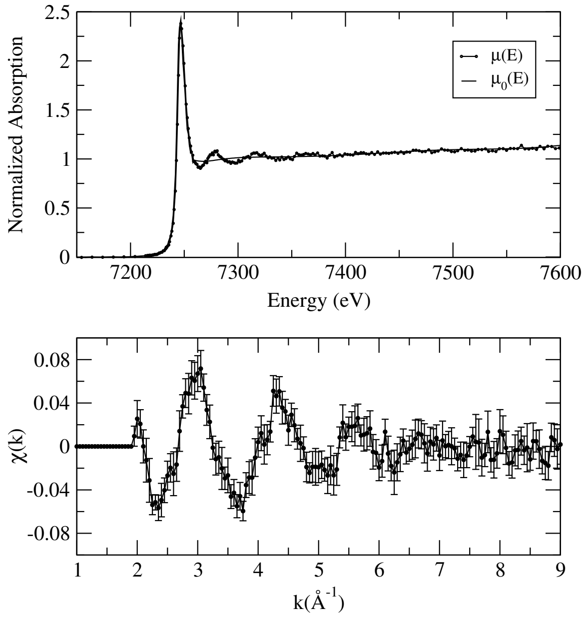

FIG. 1. Top: Step-normalized raw absorption data at the Gd L_3 edge of $Gd_{0.18}Si_{0.82}$ at T=12K (points) together with the embedded atom background function (line) used to isolate the XAFS. Bottom: resultant XAFS data (points); error bars are standard deviations obtained from 12 consecutive scans.

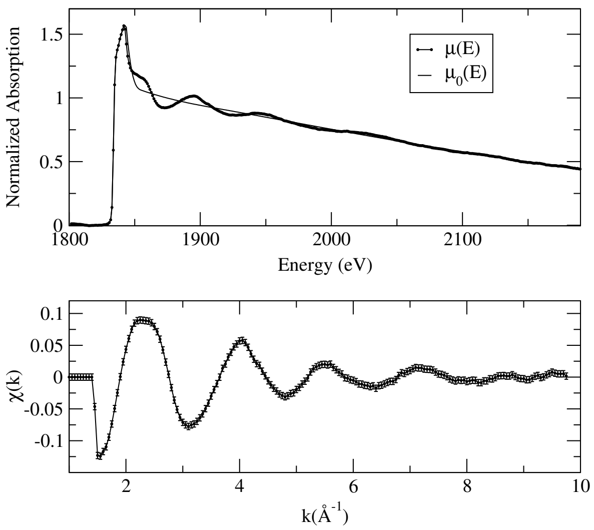

FIG. 3. Top: Step-normalized raw absorption data at the Si K edge of $Gd_{0.18}Si_{0.82}$ at T=300K (points) together with the embedded atom background function (line) used to isolate the XAFS. Bottom: resultant XAFS data (points); error bars are standard deviations obtained from 2 consecutive scans.

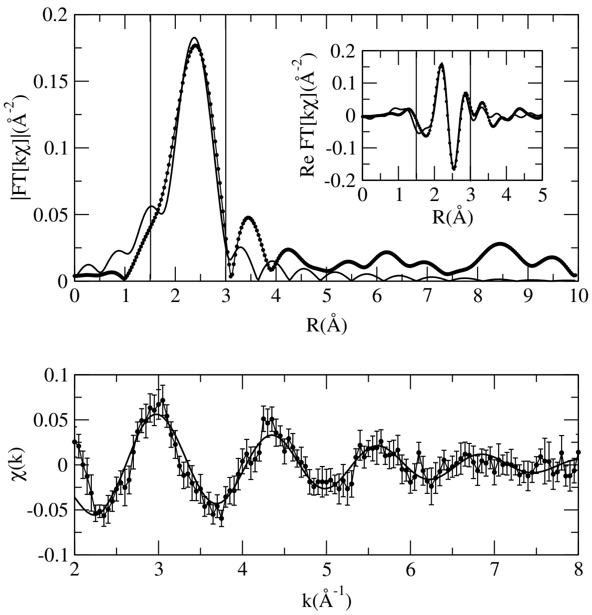

FIG. 2. Top: Magnitude and real part (inset) of the complex Fourier transform of $k\chi(k)$ for $Gd_{0.18}Si_{0.82}$ at T=12K for data (points) and fits (lines). Vertical lines delimit the fitted region of r-space. Bottom: $\chi(k)$ data (points) and fit (line) from the same sample. No significant XAFS is detected past the first coordination shell, consistent with the amorphous state of the sample.

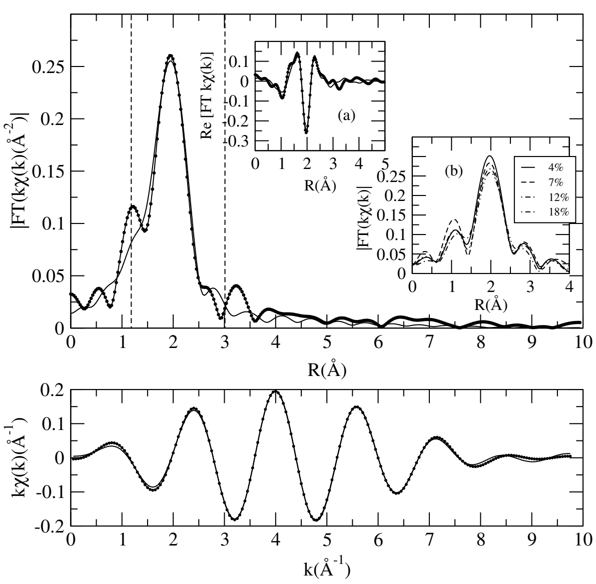

FIG. 4. Top: Magnitude (main panel) and real part (inset [a]) of the complex Fourier transform of Si K-edge $k\chi(k)$ data (points) and fits (lines) for $Gd_{0.18}Si_{0.82}$ at T=300K. Vertical lines delimit the fitted region of r-space. Inset (b) shows the decrease in XAFS amplitude with increased Gd concentration. Bottom: $k\chi(k)$ back-FT data (points) and fit (line) from the same sample.

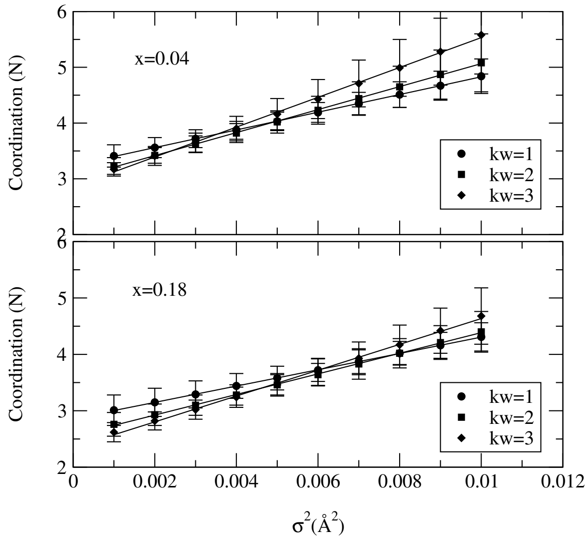

FIG. 5. The effect of correlations between N and σ^2 fitting parameters and how these correlations are changed by fitting differently weighted XAFS data; i.e., $k^w\chi(k)$. Here σ^2 is set in a finite range and N is fitted for $w = 1, 2, 3$. The physical value of N is independent of the arbitrary k-weight used in the fits.